

Quantifying memory and persistence in the atmosphere–land/ocean carbon system

Matthias Jonas¹, Rostyslav Bun^{2,3}, Iryna Ryzha², and Piotr Żebrowski¹

¹Advancing Systems Analysis Program, International Institute for Applied Systems Analysis, 2361, Laxenburg, Austria

²Department of Applied Mathematics, Lviv Polytechnic National University, 79013, Lviv, Ukraine

³Department of Transport and Computer Sciences, WSB University, 41300, Dąbrowa Górnicza, Poland

Correspondence: Matthias Jonas (jonas@iiasa.ac.at)

Abstract.

Here we intend to further the understanding of the planetary burden (and its dynamics) caused by the effect of the continued increase of carbon dioxide (CO₂) emissions from fossil fuel burning and land use and by global warming from a new, a rheological (stress-strain) perspective. That is, we perceive the emission of anthropogenic CO₂ into the atmosphere as stressor and survey the condition of Earth in stress-strain units (stress in units of Pa, strain in units of 1)—allowing access to and insight into previously unknown characteristics reflecting Earth’s rheological status. We use the idea of a Maxwell body consisting of elastic and damping (viscous) elements to reflect the overall behaviour of the atmosphere–land/ocean system in response to the continued increase of CO₂ emissions between 1850 and 2015. Thus, from the standpoint of a global observer, we see that the CO₂ concentration in the atmosphere increases (rather quickly). Concomitantly, the atmosphere warms and expands, while part of the carbon is locked away (rather slowly) in land and oceans, likewise under the influence of global warming.

It is not known how reversible and how much out of sync the latter process (uptake of carbon by sinks) is in relation to the former (expansion of the atmosphere). All we know is that the slower process remembers the influence of the faster one which runs ahead. Important questions arise as to whether this global-scale memory—Earth’s memory—can be identified and quantified, how it behaves dynamically and, last but not least, how it interlinks with persistence by which we understand Earth’s path dependency.

We go beyond textbook knowledge by introducing three parameters that characterise the system: delay time, memory, and persistence. The three parameters depend, *ceteris paribus*, solely on the system’s characteristic viscoelastic behaviour and allow deeper and novel insights into that system. The parameters come with their own limits which govern the behaviour of the atmosphere–land/ocean carbon system, independently from any external target values (such as temperature targets justified by means of global change research). We find that since 1850, the atmosphere–land/ocean system has been trapped progressively in terms of persistence (i.e., it will become progressively more difficult to relax the system), while its ability to build up memory has been reduced. The ability of a system to build up memory effectively can be understood as its ability to respond still within its natural regime; or, if the build-up of memory is limited, as a measure for system failures globally in the future. Approximately 60% of Earth’s memory had already been exploited by humankind prior to 1959. Based on these stress-strain

- 25 insights we expect that the atmosphere–land/ocean carbon system is forced outside its natural regime well before 2050 if the current trend in emissions is not reversed immediately and sustainably.

Keywords. Global carbon cycle, global atmosphere–land/ocean system, atmospheric CO₂ emissions, stress-strain model, Maxwell body, memory, persistence

Acronyms and Nomenclature

- 30 If terms or symbols are used in more than one way, we make them unambiguous by specifying (in parentheses) how they are used in the paper (e.g., CO₂ as chemical formula in the text or as physical parameter in units of ppmv in mathematical equations). As a basic rule, physical parameters are always specified by their units.

ad	adiabatic
C	carbon
comb	combined
CO ₂	carbon dioxide (chemical formula)
CO ₂	atmospheric CO ₂ concentration (in ppmv; parameter)
D	damping constant (in Pa y)
DIC	dissolved inorganic carbon (in $\mu\text{mol kg}^{-1}$)
E	Young's modulus (in Pa)
GHG	greenhouse gas
h	altitude (in m)
it	isothermal
K	compression modulus (in Pa)
L	land (index)
L	leaf-level factor (in ppmv ⁻¹ ; parameter)
M	memory (in units of 1)
MB	Maxwell body
n.a.	not assessable
NPP	net primary productivity/production (in PgC y ⁻¹)
O	oceans
p	atmospheric pressure (in hPa)
pCO ₂	partial pressure of atmospheric CO ₂ (in μatm)
P	persistence (in units of 1)
Ph	global photosynthetic carbon influx (in PgC y ⁻¹)
q	auxiliary quantity (in units of 1)
R	Revelle (buffer) factor (in units of 1)

SD	supplementary data
SE	sensitivity experiment
SI	supplementary information
t	time (in y)
T	delay time (in units of 1)
TOA	top of the atmosphere
w	weight(ed)
α	exponential growth factor of the strain (in y^{-1})
α_{ppm}	exponential growth factor of the atmospheric CO_2 concentration (in y^{-1})
β	auxiliary quantity (in units of 1)
β_b	biotic growth factor (in units of 1)
β_{Ph}	photosynthetic beta factor (in units of 1)
ε	strain (referring to atmospheric expansion by volume and CO_2 uptake by sinks; in units of 1)
γ	isentropic coefficient of expansion (in units of 1)
κ	compressibility (in Pa^{-1})
σ	stress (atmospheric CO_2 emissions from fossil fuel burning and land use; in Pa)

1 Motivation

Over the last century anthropogenic pressure on Earth became increasingly noticeable. Human activities turned out to be so pervasive and profound that the very life support system upon which humans depend is threatened (Steffen et al., 2004, 2015). The increase of emissions of greenhouse gases (GHGs) into the atmosphere is only one of several serious global threats and their reduction is in the center of international agreements (Steffen et al., 2015; UN Climate Change, 2022; UN Sustainable Development Goals, 2022).

Here we intend to further the understanding of the planetary burden (and its dynamics) caused by the effect of the continued increase of GHG emissions and by global warming from a new, a rheological (stress-strain) perspective. That is, we perceive the emission of anthropogenic GHGs, notably carbon (CO_2), into the atmosphere as stressor. This perspective goes beyond the global carbon mass-balance perspective applied by the carbon community, which is widely referred to as the gold standard in assessing whether Earth remains hospitable for life (Global Carbon Project, 2019). There, the condition of Earth is surveyed in units of $PgC\ y^{-1}$, while we survey its condition in stress-strain units (stress in units of Pa, strain in units of 1)—allowing access to and insight into previously unknown characteristics reflecting Earth’s rheological status.

We note that—although the focus is on the atmosphere–land/ocean carbon system—the stress-strain approach described herein should not be considered as an appendix to a mass-balance based carbon cycle model. Instead, it leads to a self-standing model belonging to the suite of reduced but still insightful models (such as radiation transfer, energy balance or box-type

carbon cycle models), which offer great benefits in safeguarding complex three-dimensional climate/global change models. A stress-strain model is missing in that suite of support models. Here we demonstrate the applicability and efficacy of such a model in an Earth systems context.

To develop a stress-strain systems perspective, we begin with the stress given by the CO₂ emissions from fossil fuel burning and land use between 1959 and 2015 (with the increase between 1850 and 1958 serving as antecedent or upstream emissions). Thus, from the standpoint of a global observer, we see that the CO₂ concentration in the atmosphere increases (rather quickly). Concomitantly, the atmosphere warms (here combining the effect of tropospheric warming and stratospheric cooling) and expands (by approximately 15–20 m in the troposphere per decade since 1990), while part of the carbon is locked away (rather slowly) in land and oceans, likewise under the influence of global warming (Global Carbon Project, 2019; Lackner et al., 2011; Philipona et al., 2018; Steiner et al., 2011, 2020). We refer to these two processes together, the expansion of the atmosphere and the uptake of carbon by sinks, as the overall strain response of the atmosphere–land/ocean carbon system.

It is not known how reversible and how much out of sync the latter process (uptake of carbon by sinks) is in relation to the former (expansion of the atmosphere) (Boucher et al., 2012; Dusza et al., 2020; Garbe et al., 2020; Schwinger and Tjiputra, 2018; Smith, 2012). All we know is that the slower process remembers the influence of the faster one which runs ahead. Three (nontrivial) questions arise: (1) Can this global-scale memory—Earth’s memory—be quantified? (2) Can Earth’s memory be compared with a buffer which is limited and negligently exploited; that is, what is the degree of depletion? And (3) does Earth’s memory allow its persistence (path dependency) to be quantified, speculating that the two are not independent of each other? We answer these questions in the course of our paper.

This suggests, as the next step in developing a stress-strain systems perspective, getting a grip on Earth’s memory. To this end, we focus on the slow-to-fast temporal offset inherent in the atmosphere–land/ocean system, while preferring an approach which is reduced to the highest possible extent; however, without compromising complexity in principle. To this end, it is sufficient to resolve subsystems as a whole and to perceive their physical reaction in response to the increase in atmospheric CO₂ concentrations as a combined one (i.e., including effects such as that of global warming). From a temporal perspective, the subsystems’ reactions, the expansion of the atmosphere by volume and the sequestration of carbon by sinks, can be considered sufficiently disjunct. Under optimal conditions (referring to the long-term stability of the temporal offset), the temporal-offset view even suggests that we can refrain from disentangling the exchange of both thermal energy and carbon throughout the atmosphere–land/ocean system, as it is done in climate-carbon models ranging from reduced to complex (Flato et al., 2013; Harman and Trudinger, 2014). The additional degree of reductionism, whilst preserving complexity, will prove an advantage in advancing our understanding of the temporal offset in terms of memory and persistence.

In view of the aforementioned questions, we chose a rheological stress-strain (σ - ε) model (Roylance, 2001; TU Delft, 2021); here a Maxwell body (MB) consisting of an elastic element (its constant, traditionally denoted E [Young’s modulus], is replaced by the compression modulus K) and a damping (viscous) element (the damping constant is denoted D), to capture the stress-strain behaviour of the global atmosphere–land/ocean system (Fig. 1) and to simulate how humankind propelled that global-scale experiment historically. We note that the MB is a logical choice of model given the uninterrupted increase in atmospheric CO₂ concentrations since 1850 (Global Carbon Project, 2019).

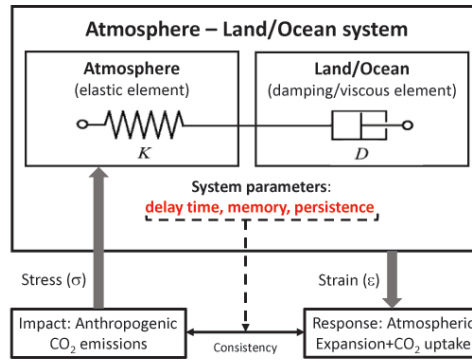


Figure 1. Rheological model to capture the stress-strain behavior of the global atmosphere–land/ocean system as a Maxwell body, consisting of elastic (atmosphere) and damping/viscous (land/ocean) elements. The stress (in units of Pa; known) is given by the carbon (CO₂) emissions from fossil fuel burning and land use, while the strain (in units of 1; assumed exponential, otherwise unknown) is given by the expansion of the atmosphere by volume and uptake of CO₂ by sinks. Independent estimates of K and D , the compression and damping characteristics of the MB, allow its stress-strain behaviour to be captured and adjusted until consistency is achieved (see text).

In practice, rheology is principally concerned with extending continuum mechanics to characterise the flow of materials that exhibit a combination of elastic, viscous, and plastic behaviour (that is, including hereditary behaviour) by properly combining elasticity and (Newtonian) fluid mechanics. Limits (e.g., viscosity limits) exist beyond which basic rheological models are recommended to be refined. However, these limits are fluent, and basic rheological models also produce useful results beyond these limits (Malkin and Isayev, 2017; Mezger, 2006; TU Delft, 2021).

The mathematical treatment of a MB is standard. Depending on whether the strain (ε) or the stress (σ) is known (in addition to the compression and damping characteristics K and D), the stress-strain equation describing the MB between 0 and t can be applied in a stress-explicit form

$$\sigma(t) = \sigma(0) \exp\left(-\frac{K}{D}t\right) + K \int_0^t \dot{\varepsilon}(\tau) \exp\left(-\frac{K}{D}(\tau - t)\right) d\tau \quad (1a)$$

or in a strain-explicit form

$$\varepsilon(t) = \varepsilon(0) + \frac{1}{K} [\sigma(t) - \sigma(0)] + \frac{1}{D} \int_0^t \sigma(\tau) d\tau \quad (1b)$$

with $\sigma(0)$ and $\varepsilon(0)$ denoting initial conditions and a dot the derivative by time (Roynance, 2001; Bertram and Glüge, 2015).

Here, we focus on the application of these equations in an atmosphere–land/ocean carbon context. For an observer it is the overall strain response of that system (expansion of the atmosphere by volume and uptake of CO₂ by sinks) that is unknown. However, since atmospheric CO₂ concentrations have been observed to increase exponentially (quasi continuously), the strain can be expected to be exponential or close to exponential. In addition, we provide independent estimates of the likewise

100 unknown compression and damping characteristics of the MB. This a priori knowledge allows equations (1a) and (1b) to be used stepwise in combination to narrow down our initial estimate of the K/D ratio, in particular. More accurate knowledge of this ratio is needed when we go beyond textbook knowledge by distilling three parameters—delay time (reflecting the temporal offset mentioned above), memory, and persistence—from the stress-explicit equation. The three parameters depend, ceteris paribus, solely on the system’s characteristic K/D ratio and allow deeper and novel insights into that system. We see
105 the atmosphere–land/ocean system as being trapped progressively over time in terms of persistence. Given its reduced ability to build up memory, we expect system failures globally well before 2050 if the current trend in emissions is not reversed immediately and sustainably. Put differently, the stress-strain approach comes with its own internal limits which govern the behaviour of the atmosphere–land/ocean carbon system, independently from any external target values (such as temperature targets justified by means of global change research).

110 There exists a wide range of other approaches which aim at exploring memory and persistence in Earth systems data, typically with the focus on individual Earth subsystems or processes (e.g., atmospheric temperature or carbon dioxide emissions). So far, applied approaches are mainly based on classical time-series and time-space analyses to uncover the memory or causal patterns contained in observational data (Barros et al., 2016; Belbutte and Pereira, 2017; Caballero et al., 2002; Franzke, 2010; Lüdecke et al., 2013). However, these approaches come with well-known limitations which can all be attributed, directly or
115 indirectly, to the issue of forecasting (more precisely, the conditions placed on the data to enable forecasting) or are not based on physics (Aghabozorgi et al., 2015; Darlington, 1996; Darlington and Hayes, 2016). By way of contrast, we do not forecast. We perpetuate long-term historical conditions which, in turn, allows the delay time in the atmosphere–land/ocean system to be expressed analytically in terms of memory and persistence. We are not aware of any scientific discipline or research area where memory and persistence are defined other than statistically and are interlinked, if at all, other than via correlation.

120 Rheological approaches are common in Earth systems modelling as well. Typically, they are applied to mimic the long(er)-term behaviour of Earth subsystems, e.g. its mantle viscosity which is crucial for interpreting glacial uplift resulting from changes in planetary ice sheet loads (Müller, 1986; Whitehouse et al., 2019; Yuen et al., 1986). Yet, to the best of our knowledge, a rheological approach to unravel the memory-persistence behaviour of the global atmosphere–land/ocean system in response to the long-lasting increase in atmospheric CO_2 emissions had not been applied before.

125 We describe our rheological model (MB) approach in detail in Section 2, while we provide an overview of the applied data and conversion factors in Section 3. In Section 4 we describe how we derive first-order estimates of the main characteristics of the atmosphere–land/ocean system (in terms of the MB’s K and D characteristics) by using available knowledge. Although uncertain, these estimates come useful in Section 5 where we apply the aforementioned stress and strain explicit equations to quantify delay time, memory, and persistence of the atmosphere–land/ocean system. We conclude by taking account of our
130 main findings in Section 6.

2 Method

This section provides an overview of how we process equation (1a), and how we distil delay time, memory, and persistence from this equation. To familiarise oneself with the details, the reader is referred to the Supplementary Information.

To start with, we assume that we know the order of magnitude of both the K/D ratio characteristic of the atmosphere–land/ocean system and the rate of change in the strain ε given by $\dot{\varepsilon}(t) = \alpha \exp(\alpha t)$ with the exponential growth factor $\alpha > 0$. These first-order estimates permit equations (1a) and (1b) to be used stepwise in combination:

Equation (1a): We vary both K/D and α to reproduce the known stress σ given by the CO₂ emissions from fossil fuel burning (fairly well known) and land use (less known) (Global Carbon Project, 2019).

Equation (1b): We insert both the fine-tuned K/D ratio and the known stress σ to compute the strain ε and check its derivative by time.

We consider this procedure a check of consistency, not a proof of concept.

Delay time, memory, and persistence are characteristic (functions) of the MB. They are contained in the integral on the right side of equation (1a) and are defined independently of initial conditions. These appear only in the lower boundary of that integral which allows initial conditions other than zero to be considered by taking advantage of the integral’s additivity. Thus, without loss of generality, we rewrite equation (1a) for $\sigma(0) = 0$, which results in

$$\sigma(t) = \frac{D}{\beta} \dot{\varepsilon}(t) (1 - q_\beta^t) \quad (2a)$$

(see Supplementary Information 1), where $\beta = 1 + \frac{D}{K}\alpha$ and $q_\beta^t = \exp(-\frac{K}{D}\beta t)$. The term $\frac{D}{K\beta}$ represents a time characteristic of the MB under (here) exponential strain (i.e., of the MB that responds to the stress acting upon it), whereas $\frac{D}{K}$ is the relaxation time of the MB (i.e., of the MB that relaxes unhindered after the stress causing that strain has vanished, or that responds to strain held constant over time; also known as the relaxation test (Bertram and Glüge, 2015)). However, to ensure that exponents still come in units of 1 after we split them up, we introduce the dimensionless time $n = \frac{t}{\Delta t}$ globally (which will be discretised in the sequel when we refer to a temporal resolution of 1 year and set $\Delta t = 1$ y), such that, for example, $q^t = \exp(-\frac{K}{D}\Delta t)^n$.

To understand the systemic nature of the MB, we explore its stress dependence on $q = \exp(-\frac{K}{D}\Delta t)$, which contains the ratio of K and D , the two characteristic parameters of the MB, by way of derivation by q (while α is held constant). To this end, we transform equation (2a) further to

$$\sigma_D(q, t) := \frac{1}{D} \sigma(t) = \frac{1}{D} \sigma(n) =: \sigma_D(q, n) \quad (2b)$$

and execute $\frac{\partial}{\partial q} \sigma_D(q, n)$, the derivation by q of the system’s rate of change σ_D (which is given in units of y^{-1}). Doing so allows (what we call) delay time T to be distilled (see Supplementary Information 2). It is defined as

$$T(q, n) := \frac{q_\beta}{S_n} \frac{\partial S_n}{\partial q_\beta} = -\frac{q_\beta^n}{1 - q_\beta^n} n + \frac{q_\beta}{1 - q_\beta}, \quad (3)$$

where $q_\beta = q_\alpha q$, $q_\alpha = \exp(-\alpha \Delta t)$, and $S_n = S(q, n) = \frac{1 - q_\beta^n}{1 - q_\beta}$. The delay time behaves asymptotically for increasing n and approaches $T_\infty = \lim_{n \rightarrow \infty} T = \frac{q_\beta}{1 - q_\beta}$. We further define

$$M := S(q, n) \quad (4)$$

with $M_\infty := \frac{1}{1-q_\beta}$ and

$$P := T(q, n)^{-1} \tag{5}$$

165 with $P_\infty := \frac{1}{T_\infty} = \frac{1-q_\beta}{q_\beta}$ as the MB's characteristic memory and persistence, respectively. As is commonly done, we keep the list of independent parameters minimal. (We only allow K and D [i.e., q] in addition to n ; see equations [2b] and [3]–[5], in particular.)

T as given by equation (3) is not simply characteristic of the MB described by equation (2); it can be shown to appear as delay time in the argument of any function dependent on current and previous times, with a weighting decreasing exponentially backward in time (see Supplementary Information 3). Equation (4) reflects the history the MB was exposed to systemically prior to current time n (during which α was constant; see Supplementary Information 4). Put simply, M can be understood as the depreciated (q -weighted) strain summed up backward in time. Equation (5) can be shortened to $T \cdot P = 1$. If we assume that q can be changed in retrospect at $n = 0$, this equation tells us that if T —that is, ΔM per Δq (or, likewise, $\Delta M/M$ per $\Delta q/q$; see the first part of equation [3])—is small, P is great because the change in the system's characteristics (contained in 175 q) hardly influences the MB's past, with the consequence that the past exhibits a great path dependency, and vice versa. We therefore perceive persistence and path dependency as synonymous.

An additional quantity to monitor is $\ln(M \cdot P)$, which approaches $\lambda_\beta = \lambda \cdot \beta$ for increasing n with $\lambda = \frac{K}{D} \Delta t$ the characteristic rate of change in the MB. The ratio $\lambda / \ln(M \cdot P)$ allows monitoring of how much the system's natural rate of change is exceeded as a consequence of the continued increase in stress (see Supplementary Information 5).

180 3 Data and Conversion Factors

A detailed overview of the carbon data and conversion factors used in this paper (and also by the carbon community) is given in Supplementary Information 6. The data pertain to atmosphere, land, and oceans,

- atmospheric CO₂ concentration (in ppm)
- CO₂ emissions from fossil-fuel combustion and cement production (in PgC y⁻¹)
- 185 – land-use change emissions (in PgC y⁻¹)
- net primary production (in PgC y⁻¹)
- dissolved organic carbon (in $\mu\text{mol kg}^{-1}$);

and are given by source and time range and are also described briefly. The context within which they are used is revealed in each of the following sections. The conversion factors are standard; they are needed to convert C to CO₂, and ppmv CO₂ to 190 PgC or Pa.

4 Independent Estimates of D and K

In this section we provide independent estimates of the damping and compression characteristics of the atmosphere–land/ocean system, with D_L and D_O denoting the damping constants assigned to land and oceans, respectively, and K denoting the compression modulus assigned to the atmosphere. We capture the characteristics’ right order of magnitude only—which can
195 be done on physical grounds by evaluating the combined (net) strain response of each subsystem on grounds of increasing CO_2 concentrations in the atmosphere. These first-order estimates are adequate as they allow sufficient flexibility for Section 5, where we narrow down our initial estimates by using equations (1a) and (1b) stepwise in combination to achieve consistency.

4.1 Estimating the Damping Constant D_L

Increasing concentrations of CO_2 in the atmosphere trigger the uptake of carbon by the terrestrial biosphere. The intricacies of
200 this process, including potential (positive and negative) feedback processes, are widely discussed (Dusza et al., 2020; Heimann and Reichstein, 2008; Smith, 2012). The crucial question is how we have observed the process of carbon uptake by the terrestrial biosphere taking place in the past. Compared to the reaction of the atmosphere to global warming (an expansion of the atmosphere by volume), we consider this process to be long(er) term in nature and perceive it as a Newton-like (damping) element.

205 Biospheric carbon uptake is described by the biotic growth factor

$$\beta_b = \frac{\Delta NPP/NPP}{\Delta \text{CO}_2/\text{CO}_2} \quad (6)$$

which is used to approximate the fractional increase in net primary productivity (NPP) per unit increase in atmospheric CO_2 concentration (Wullschlegel et al., 1995; Amthor and Koch, 1996; Luo and Mooney, 1996). Here we make use of the model-derived NPP time series (1900–2016) provided by O’Sullivan et al. (2019) to calculate β_b (O’Sullivan et al., 2019).
210 To understand the uncertainty range underlying β_b for 1959–2018, we use the photosynthetic beta factor

$$\beta_{Ph} = \text{CO}_2 L = \left(\frac{dPh}{Ph} \right) \left(\frac{\text{CO}_2}{d\text{CO}_2} \right) \quad (7)$$

where L is the so-called leaf-level factor denoting the relative leaf photosynthetic response to a 1 ppmv change in the atmospheric concentration of CO_2 , bounded by

$$L_1 \leq L = f(\text{CO}_2) \leq L_2, \quad (8)$$

215 (see below); and Ph is the global photosynthetic carbon influx (i.e., gross primary productivity). Equation (7) is similar to equation (6). In equation (6) β_b represents biomass production changes in response to CO_2 changes, whereas in equation (7) β_{Ph} describes photosynthesis changes in response to CO_2 changes (Luo and Mooney, 1996).

L can be shown to be independent of plant characteristics, light, and the nutrient environment and to vary little by geographic location or canopy position. Thus, L is virtually a constant across ecosystems and a function of time-associated changes in
220 atmospheric CO_2 only (Luo and Mooney, 1996).

We use equation (7) to test whether β_b falls within the range of β_{Ph} given by the quantifiable photosynthetic limits L_1 (photosynthesis limited by electron transport) and L_2 (photosynthesis limited by rubisco activity). Fig. 2 shows the biotic growth factors from O’Sullivan et al. that consider changes in NPP due to the combined effect of CO_2 fertilisation, nitrogen deposition, climate change, and carbon–nitrogen synergy (β_{NPP_comb}) and due to CO_2 fertilisation ($\beta_{NPP_CO_2}$) only. For 1960–2016, β_{NPP_comb} falls in between $\beta_1 := \beta_{Ph}(L_1)$ and $\beta_2 := \beta_{Ph}(L_2)$, closer to β_1 than to β_2 , whereas $\beta_{NPP_CO_2}$ falls even below the lower β_1 limit.

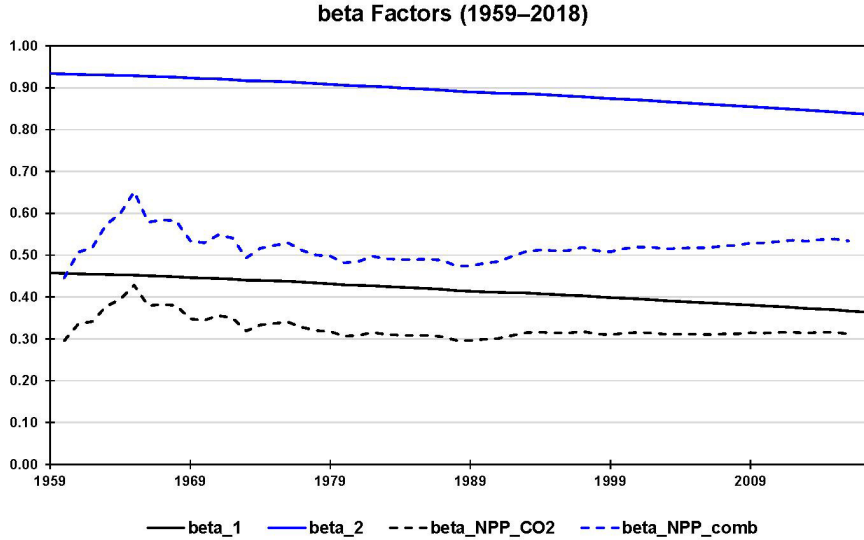


Figure 2. Using the lower (β_1) and upper (β_2) limits of the photosynthetic beta factor to test the range of the biotic growth factor (β_b) for 1960–2016. The biotic growth factor is derived with the help of modelled net primary production (NPP) values accounting for CO_2 fertilisation, nitrogen deposition, climate change, and carbon–nitrogen synergy. $\beta_{NPP_CO_2}$ refers to O’Sullivan et al. (2019), who consider the change in NPP due to CO_2 fertilisation only, and β_{NPP_comb} refers to the change in NPP due to the combined effect. All beta factors are in units of 1.

Rewriting equation (7) in the form

$$\frac{\Delta Ph_i}{Ph} = L_i \Delta CO_2 \quad (i = 1, 2) \quad (9)$$

with $Ph = 120 \text{ PgC y}^{-1}$ indicates that the additional amount of annual relative photosynthetic carbon influx, stimulated by a yearly increase in atmospheric CO_2 concentration, can be estimated by L_i , or the sequence of L_i if ΔCO_2 spans multiple years (see Supplementary Information 7 and Supplementary Data 1). Plotting $\Delta Ph_i / Ph$ against time allows lower and upper slopes (rates of strain)

$$\frac{d}{dt} \left(\frac{\Delta Ph_1}{Ph} \right) \approx 0.0019 \text{ y}^{-1} \quad (10a)$$

and

$$235 \quad \frac{d}{dt} \left(\frac{\Delta Ph_2}{Ph} \right) \approx 0.0041 y^{-1} \quad (10b)$$

to be derived for 1959–2018. A linear fit works well in either case. The cumulative increase in atmospheric CO_2 concentration since 1959, $\Delta CO_2 = CO_2(t) - CO_2(1959)$, exhibits a moderate exponential (close to linear) trend. Thus, plotting annual changes in CO_2 , normalised on the aforementioned rates of strain, versus time allows the remaining (moderate) trends to be interpreted alternatively, namely, as average photosynthetic damping constants with appropriate uncertainty given by half the
240 maximal range (see Fig. 3 and Supplementary Data 1)

$$D_1 \approx (815 \pm 433) \text{ ppmv y} = (83 \pm 44) \text{ Pa y} = (2606 \pm 1383) 10^6 \text{ Pa s} \quad (11a)$$

$$D_2 \approx (378 \pm 201) \text{ ppmv y} = (38 \pm 20) \text{ Pa y} = (1207 \pm 641) 10^6 \text{ Pa s} \quad (11b)$$

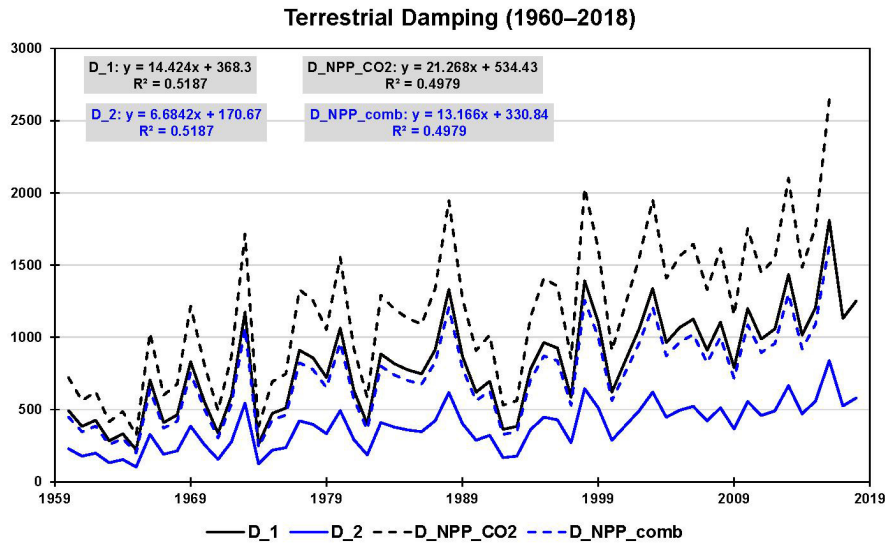


Figure 3. Terrestrial carbon uptake perceived as damping (in ppmv y) based on the limits of leaf photosynthesis (1960–2018: D_1 and D_2) and on model-derived changes in net primary production (NPP ; 1960–2016) due to both the combined effect of CO_2 fertilisation, nitrogen deposition, climate change, and carbon–nitrogen synergy (D_{NPP_comb}) and CO_2 fertilisation only ($D_{NPP_CO_2}$). The linear trends of the four damping series are shown at the top. These are used to interpret damping as constants with appropriate uncertainty (given by half the maximal range).

Repeating the same procedure for 1959–2016 with O’Sullivan et al.’s model-derived NPP values considering the change in NPP due to CO_2 fertilisation as well as the total change in NPP , we find

$$245 \quad \frac{d}{dt} \left(\frac{\Delta NPP}{NPP} \right)_{CO_2} \approx 0.0013 y^{-1} \quad (12a)$$

and

$$\frac{d}{dt} \left(\frac{\Delta NPP}{NPP} \right)_{comb} \approx 0.0021 y^{-1} \quad (12b)$$

(linear fits still work well); and consequently

$$D_{CO_2} \approx (1172 \pm 617) \text{ ppmv y} = (119 \pm 62) \text{ Pa y} = (3746 \pm 1971) 10^6 \text{ Pa s} \quad (13a)$$

$$250 \quad D_{comb} \approx (726 \pm 382) \text{ ppmv y} = (74 \pm 39) \text{ Pa y} = (2319 \pm 1220) 10^6 \text{ Pa s}. \quad (13b)$$

As before, these estimates are closer to the lower leaf-level factor (higher photosynthetic D) than to the higher leaf-level factor (lower photosynthetic D ; Fig. 3).

Here we interpret O’Sullivan et al.’s Earth systems model as a typical one, which means that the NPP changes it produces are common. We therefore (and sufficient for our purposes) choose the damping constant D_1 as a good estimator in light of the
 255 total change in NPP of the terrestrial biosphere since 1960. Hence

$$D_L \approx (815 \pm 433) \text{ ppmv y} = (83 \pm 44) \text{ Pa y} = (2606 \pm 1383) 10^6 \text{ Pa s}. \quad (14)$$

D_L is on the order of viscosity indicated for bitumen/asphalt (Mezger, 2006).

4.2 Estimating the Damping Constant D_O

Increasing concentrations of CO_2 in the atmosphere trigger the uptake of carbon by the oceans (National Oceanic and Atmospheric Administration, 2015). Like the uptake of carbon by the terrestrial biosphere, we consider this process to behave like
 260 a Newton (damping) element in our MB because of the de-facto irreversibility on the shorter time scale we are interested in (Schwinger and Tjiputra, 2018).

The Revelle (buffer) factor (R) quantifies how much atmospheric CO_2 can be absorbed by homogeneous reaction with seawater. R is defined as the fractional change in CO_2 relative to the fractional change in dissolved inorganic carbon (DIC):

$$265 \quad R = \frac{\Delta pCO_2 / pCO_2}{\Delta DIC / DIC}. \quad (15)$$

(Here, in contrast to before, atmospheric CO_2 is referred to in units of μatm and therefore indicated by pCO_2 .) An R value of 10 indicates that a 10% change in atmospheric CO_2 is required to produce a 1% change in the total CO_2 content of seawater (Bates et al., 2014; Egleston et al., 2010; Emerson and Hedges, 2008).

DIC and R have been observed at seven ocean carbon time-series sites for periods from 15 to 30 years (between 1983 and
 270 2012) to change slowly and linearly with time (Bates et al., 2014):

$$\frac{\Delta DIC}{\Delta t} \approx [0.8; 1.9] \mu\text{mol kg}^{-1} \text{y}^{-1} \quad (16)$$

$$\frac{\Delta R}{\Delta t} \approx [0.01; 0.03] \text{y}^{-1} \quad (17)$$

(see also Supplementary Data 2). Here it is sufficient to proceed with spatiotemporal averages. As before, the cumulative increase in atmospheric CO_2 concentration since 1983, $\Delta p\text{CO}_2 = p\text{CO}_2(t) - p\text{CO}_2(1983)$, exhibits a moderate exponential (close to linear) trend. Thus, plotting annual changes in $p\text{CO}_2$, normalised on the rates of strain $\frac{(\Delta\text{DIC}/\text{DIC})}{\Delta t}$, versus time allows the remaining (moderate) trend to be interpreted alternatively, namely, as an average oceanic damping constant with appropriate uncertainty given by half the maximal range (see Fig. 4 and Supplementary Data 2):

$$D_O \approx (3005 \pm 588) \text{ ppmv y} = (304 \pm 60) \text{ Pa y} = (9602 \pm 1877) 10^6 \text{ Pa s.} \quad (18)$$

D_O is on the order of viscosity indicated for bitumen/asphalt, yet approximately 3.7 times greater than D_L .

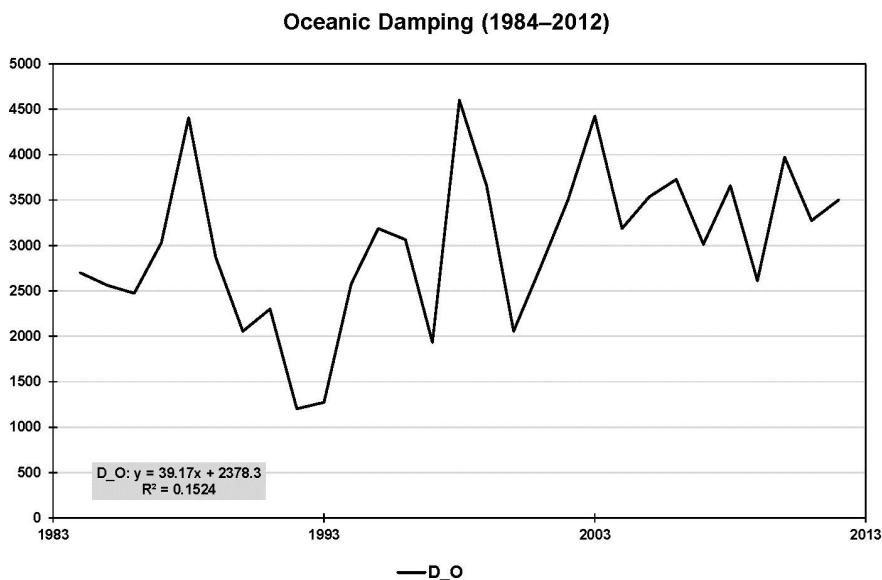


Figure 4. Oceanic carbon uptake perceived as damping (in ppmv y) based on observations at seven ocean carbon time-series sites for periods from 15 to 30 years (between 1983 and 2012). The linear trend in oceanic damping, shown at the bottom, is used to interpret damping as a constant with appropriate uncertainty (given by half the maximal range).

4.3 Estimating the Compression Modulus K

The long-lasting increase in GHG emissions has caused the CO_2 concentration in the atmosphere to increase and the atmosphere as a whole to warm (with tropospheric warming outstripping stratospheric cooling) and to expand (in the troposphere by approximately 15–20 m per decade since 1990) (Global Carbon Project, 2019; Lackner et al., 2011; Philipona et al., 2018; Steiner et al., 2011, 2020). Our whole-subsystem (net-warming) view does not invalidate the known facts that CO_2 in the atmosphere is well-mixed (except for very low altitudes where deviations from uniform CO_2 concentrations are caused by the dynamics of carbon sources and sinks) and that the volume percentage of CO_2 in the atmosphere stays almost constant up to high altitudes (Abshire et al., 2010; Emmert et al., 2012).

Compared to the slow uptake of carbon by land and oceans, we assume the atmosphere to be represented well by a Hooke
 290 element in the MB and this to serve as a (sufficiently stable) surrogate physical descriptor for the reaction of the atmosphere as a
 whole (Sakazaki and Hamilton, 2020). However, in the case of a gas, Young’s modulus E must be replaced by the compression
 modulus K , the reciprocal of which is compressibility κ . Both K and κ scale with altitude which we get to grips with in the
 following. Compressibility is defined by

$$\kappa = \frac{1}{K} = -\frac{1}{V} \frac{dV}{dp} \quad (19)$$

295 ($\kappa > 0$) (OpenStax, 2020). Depending on whether the compression happens under isothermal or adiabatic conditions, the
 compressibility is distinguished accordingly. It is defined by

$$\kappa_{it} = \frac{1}{p} \quad (20a)$$

in the isothermal case and

$$\kappa_{ad} = \frac{1}{\gamma p} \quad (20b)$$

300 in the dry adiabatic case, where γ is the isentropic coefficient of expansion. Its value is 1.403 for dry air (1.310 for CO_2) under
 standard temperature (273.15 K) and pressure (1 atm; 101.325 kPa) (Wark, 1983). We consider a carbon-enriched atmosphere
 also as air.

However, the observed expansion of the troposphere happens neither isothermally nor dry-adiabatically but polytropically.
 Moreover, our ignorance of the exact value of κ is overshadowed by the uncertainty in altitude—or top of the atmosphere
 305 (TOA)—which we need as a reference for κ (thus K). As a matter of fact, there exists considerable confusion as to which
 altitude the TOA refers in climate models (CarbonBrief, 2018; NASA Earth Observatory, 2006).

To advance, we refer to the (dry adiabatic) standard atmosphere, which assigns a temperature gradient of $-6.5^\circ\text{C}/1000\text{ m}$
 up to the tropopause at 11 km, a constant value of -56.5°C (216.65 K) above 11 km and up to 20 km, and other gradients and
 constant values above 20 km (Cavcar, 2000; Mohanakumar, 2008). Guided by the distribution of atmospheric mass by altitude,
 310 we choose the stratopause as our TOA (at about 48 km altitude and 1 hPa), with uncertainty ranging from mid-to-higher
 stratosphere (at about 43 km altitude and 1.9 hPa) to mid-mesosphere (at about 65 km altitude and 0.1 hPa) (Digital Dutch,
 1999; International Organization for Standardization, 1975; Mohanakumar, 2008; Zellner, 2011). We assign the resulting
 uncertainty of 90% in relative terms to

$$K = (1 \pm 0.9) \text{ hPa} = (100 \pm 90) \text{ Pa}, \quad (21)$$

315 which we consider sufficiently large to compensate for the unknown isentropic coefficient in the first place; that is,
 $[K_{ad,min}; K_{ad,max}] \in [K_{it,min}; K_{ad,max}] \in [K_{min}; K_{max}]$. For comparison, K_{ad} ranges from 400 to 412 hPa were the TOA
 allocated within the troposphere (exhibiting, the reference used here, an expansion of 20 m; see Supplementary Information 8).

5 Main Findings

Equation (1a) (or [2a], respectively) and equation (1b) are used stepwise in combination to conduct three sets of stress-strain
320 experiments including sensitivity experiments (SEs):

A. for the period 1959–2015 assuming zero stress and strain in 1959,

B. for the period 1959–2015 assuming zero stress and strain in 1900, and

C. for the period 1959–2015 assuming zero stress and strain in 1850

and, ultimately, also before 1850 (i.e., zero anthropogenic stress before that date).

325 The logic of the experiments is determined by both the availability of data (see Supplementary Information 6) and the increasing complementarity from A to C (see below). The basic procedure is always the same: We insert into equation (1a) our first-order estimates of $D_L \approx (83 \pm 44) \text{ Pa y}$; $D_O \approx (304 \pm 60) \text{ Pa y}$, that is, $D = D_L + D_O \approx (387 \pm 74) \text{ Pa y}$; and $K \approx (100 \pm 90) \text{ Pa}$. At the same time, we use the growth factor $\alpha_{ppm} = 0.0043 \text{ y}^{-1}$, which reflects the exponential increase in the CO_2 concentration in the atmosphere between 1959 and 2018 (see Supplementary Data 1) as our first-order estimate for α
330 in $\dot{\varepsilon} = \alpha \exp(\alpha t)$, the rate of change in strain ε . We apply equation (1a) by varying both K/D and α to reproduce the known stress σ on the left, given by the CO_2 emissions from fossil fuel burning and land use. To restrict the number of variation parameters to two, we let K and D deviate from their respective mean values equally in relative terms (i.e., we assume that our first-order estimates exhibit equal inaccuracy in relative terms) and express α as a multiple of α_{ppm} . This is easily possible with the introduction of suitable factors (see Supplementary Data 3) that allow σ to be reproduced quickly and with sufficient
335 accuracy. The main reason this works well is that the two factors pull the two exponential functions on the right side of equation (2a)— $\dot{\varepsilon}(t)$ and $(1 - q_\beta^t)$, which determine the quality of the fit—in different directions.

To A

This is our set of reference experiments, all for the period 1959–2015. This set comprises **A.1**) a stress-explicit experiment, **A.2**) three strain-explicit experiments, and **A.3**) SEs expanding the strain-explicit experiments. The parameters α , λ , and λ_β
340 are reported in y^{-1} , as is commonly done.

To A.1: In this experiment we vary the ratio K/D (λ in Table 1) and α to reproduce the monitored stress $\sigma(t)$ on the left side of equation (2a) (see Supplementary Data 3). This tuning process (hereafter referred to as “Case 0”) allows us to test whether K and D , in particular, stay within their estimated limits, namely, $K \in [10; 190] \text{ Pa}$ and $D \in [313; 461] \text{ Pa y}$ or, equivalently, $\lambda \in [0.0217; 0.6078] \text{ y}^{-1}$. Column “Case 0” in Table 1 indicates that this case is practically identical to choosing
345 $\lambda = (10/461) \text{ y}^{-1} = 0.0217 \text{ y}^{-1}$, the smallest ratio K/D deemed possible. For Case 0 we find $K = 9.9 \text{ Pa}$ and $D = 461.5 \text{ Pa y}$ (thus, $\lambda = K/D = 0.0214 \text{ y}^{-1}$) and, concomitantly, $\alpha = 0.0247 \text{ y}^{-1}$ (thus, $\lambda_\beta = (K/D)\beta = (K/D) + \alpha = 0.0461 \text{ y}^{-1}$).

Fig. 5 reflects the result of the tuning process graphically. It shows how well the monitored stress, given by the cumulated CO_2 emissions from fossil fuel burning and land use activities since 1959, can be reproduced by equation (2a). The quality of the tuning is observed by summing the squares of differences between monitored and reproduced stress from 1959 to 2015

Table 1. Overview of parameters in experiments A.1–A.3.

Parameter		Case 0	Case 1	Case 12	Case 13	Case 2	Case 21	Case 23	Case 3	Case 31	Case 32
		stress explicit	strain explicit	sensitivity experiments Case 1		strain explicit	sensitivity experiments Case 2		strain explicit	sensitivity experiments Case 3	
K	Pa	9.9	10	10	10	100	100	100	190	190	190
D	Pa·y	461.5	461	461	461	387	387	387	313	313	313
$\lambda^{a,b}$	y^{-1}	0.0214	0.0217	0.0217	0.0217	0.2584	0.2584	0.2584	0.6078	0.6078	0.6078
λ^{-1}	y	46.8	46.1	46.1	46.1	3.87	3.87	3.87	1.65	1.65	1.65
α^a	y^{-1}	0.0247	0.0248	0.0158	0.0174	0.0158	0.0248	0.0174	0.0174	0.0248	0.0158
β	1	2.158	2.144	1.729	1.803	1.061	1.096	1.067	1.029	1.041	1.026
λ_β^a	y^{-1}	0.0461	0.0465	0.0375	0.0391	0.2742	0.2832	0.2758	0.6252	0.6236	0.6236
λ_β^{-1}	y	21.7	21.5	26.7	25.6	3.65	3.53	3.63	1.60	1.58	1.60
q_β	1	0.9549	0.9546	0.9632	0.9617	0.7602	0.7534	0.7590	0.5351	0.5312	0.5360
T_∞	1	21.19	21.02	26.19	25.10	3.17	3.05	3.15	1.15	1.13	1.16
$M_\infty = T_\infty/q_\beta$	1	22.19	22.02	27.19	26.10	4.17	4.05	4.15	2.15	2.13	2.16
$P_\infty = 1/T_\infty$	1	0.0472	0.0476	0.0382	0.0398	0.3155	0.3274	0.3176	0.8686	0.8825	0.8657
$\lambda/\lambda_\beta = 1/\beta$	%	46.3	46.6	57.8	55.5	94.2	91.2	93.7	97.2	96.1	97.5
n at $T/T_\infty = 0.5$	1	—	28	34	33	5	5	5	3	3	3
$\lambda/\ln(M \cdot P)$	%	—	5	5	5	36	36	36	54	53	54
n at $M/M_\infty = 0.5$	1	—	15	19	18	3	2	3	1	1	1
$\lambda/\ln(M \cdot P)$	%	—	4	4	4	22	21	22	n.a.	n.a.	n.a.
n at $T/T_\infty = 0.95$	1	—	98	121	116	17	17	17	8	8	8
$\lambda/\ln(M \cdot P)$	%	—	25	28	27	82	79	81	91	90	91
n at $M/M_\infty = 0.95$	1	—	64	80	77	11	11	11	5	5	5
$\lambda/\ln(M \cdot P)$	%	—	13	13	13	61	60	61	74	74	74

^a Given in y^{-1} .^b Derived for K and D deviating from their respective mean values equally in relative terms.

350 using the SUMXMY2 command in Excel. (We stopped the tuning process with the sum at about 1.400 Pa^2 , when changes in K and D became negligible, resulting in a correlation coefficient of 0.9998; see Supplementary Data 3.)

Fig. 5 also shows the parameters needed to describe the monitored stress by a second-order polynomial regression (see the grey box in the upper left corner of the figure). We have not yet used this regression but will do so in the strain-explicit experiments described next.

355 **To A.2:** We use equation (1b) with $\sigma(0) = \varepsilon(0) = 0$ and $\sigma(t) = 0.0028t^2 + 0.1811t$, the second-order polynomial regression of the monitored stress (cf. Fig. 5), to conduct three experiments (hereafter referred to as “Cases 1–3”) to explore the spread in

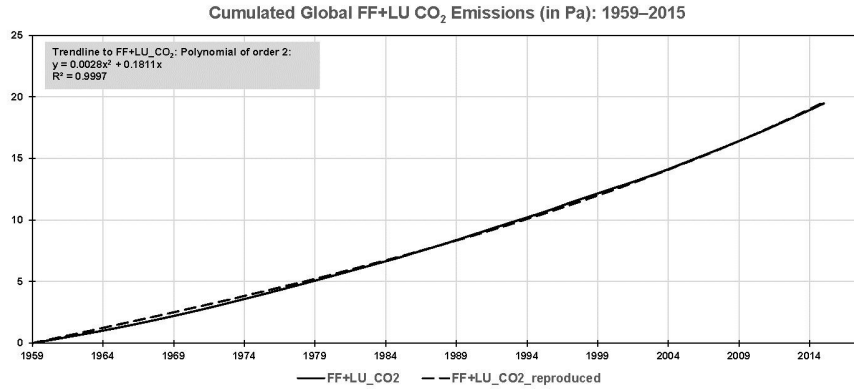


Figure 5. Case 0: K/D and α on the right side of equation (2a) are tuned to reproduce the stress $\sigma(t)$ on the left side of that equation, given by the monitored (but cumulated) CO_2 emissions from fossil fuel burning and land use activities (in Pa). The value resulting for K/D complies with its lower limit deemed possible based on the uncertainties derived for K and D in Section 4.

the strain ε . To this end, we let the ratio K/D vary from minimum (Case 1) to mean (Case 2) to maximum (Case 3; see Table 1 and Supplementary Data 4) irrespective of the outcome of the Case 0 experiment, which suggests that compared to Cases 2 and 3, Case 1 (K minimal: the atmosphere is rather compressible, D maximal: the uptake of carbon by land and oceans is rather viscous) appears to be more in conformity with reality than Cases 2 and 3.

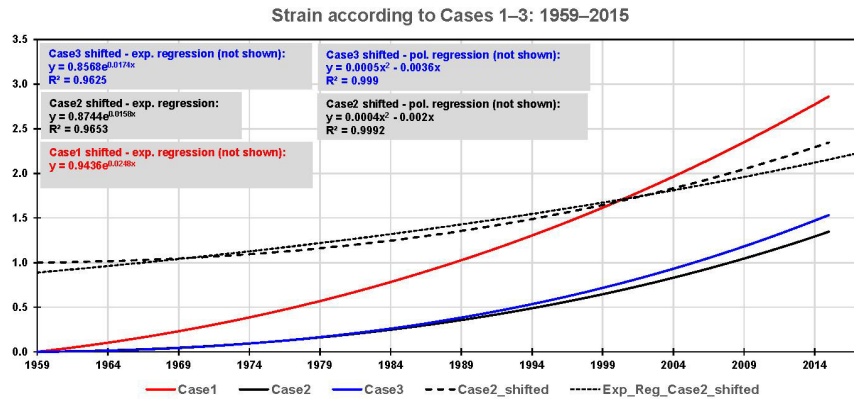


Figure 6. Cases 1–3: The ratio K/D is varied from minimum (Case 1: solid red) to mean (Case 2: solid black) to maximum (Case 3: solid blue) to explore the spread in the strain ε (in units of 1) on the left side of equation (1b), while the monitored stress is described by a second-order polynomial (see the text). These strain responses have to be shifted upward (so that they pass through 1 in 1959) to derive their rates of change, if described by an exponential regression (here only demonstrated for Case 2). As is already illustrated in Case 0, the exponential regression in Case 1 is excellent (see the text), whereas second-order polynomial regressions provide better fits in Cases 2 and 3 (see the boxes in the figure; the polynomial regressions are not shown).

Fig. 6 reflects these experiments graphically. It shows that the range of strain responses is encompassed by Case 1 ($K/D = (10/461)y^{-1}$) and Case 2 ($K/D = (100/387)y^{-1}$), not by Case 1 and Case 3 ($K/D = (190/313)y^{-1}$)—the solid blue line (Case 3) falls in between the solid red (Case 1) and solid black (Case 2) lines—resulting from how K and D dominate the individual parts of equation (1b). These strain responses have to be shifted upward (so that they pass through 1 in 1959) to describe them by an exponential regression and to derive their rates of change. The exponential fit is excellent only in Case 1, as already illustrated in Case 0 (Case 0: $\lambda = 0.0214y^{-1}$, Case 1: $\lambda = 0.0217y^{-1}$), but inferior to the polynomial regressions, here of the second order, in Cases 2 and 3. However, a second-order polynomial approach to the strain has to be discarded because the stress derived with the help of equation (1a) would exhibit a linear behaviour with increasing time and not be a polynomial of the second order as in Fig. 6 (see Supplementary Information 9).

In this regard we note that a more targeted way forward would be to use a piecemeal approach. This approach requires the data series to be sliced into shorter time intervals, during which an exponential fit for the strain (which we assume to hold in principle in deriving equation [2a] here) is sufficiently appropriate. Fortunately, as the SEs in A.3 indicate, we can hazard the consequences of using suboptimal growth factors resulting from suboptimal exponential regressions for the strain.

Equations (3) to (5) are used to determine delay time T , memory M , and persistence P (in units of 1) for Cases 1–3 as well as their characteristic limiting values T_∞ , M_∞ , and P_∞ (see Table 1 and Supplementary Data 5 to 8). We recall that T , M , and P are characteristic functions of the MB and are defined independently of initial conditions; these only specify the reference time for $n = 0$ (here 1959). Fig. 7a and 7b reflect the behaviour of T , M , and P over time (in units of 1). For a better overview, Table 1 lists the times when these parameters exceed 50% or 95%, respectively, of their limiting values (without indicating whether these levels go hand in hand with, e.g., global-scale ecosystem changes of equal magnitude). In the table we also specify the ratio $\lambda/\ln(M \cdot P)$ for each of these times (see also Fig. 7c). The ratio approaches λ/λ_β for $n \rightarrow \infty$ and indicates (as a percentage) how much smaller the system’s natural rate of change in the numerator turns out compared to the system’s rate of change in the denominator under the continued increase in stress. As is illustrated, in particular, by Case 1 in the figure, the ratio does not increase at a constant pace as n increases, which shows the nonlinear strain response of the atmosphere–land/ocean system.

To A.3: Three sets of SEs serve to assess the influence of the exponential growth factor on the strain-explicit experiments described above:

SE1: $\alpha_1 = 0.0248y^{-1}$ as in Case 1 (cf. Fig. 6) is also used in Cases 2 and 3 (hereafter referred to as “Cases 21 and 31”).

SE2: $\alpha_2 = 0.0158y^{-1}$ as in Case 2 (cf. Fig. 6) is also used in Cases 1 and 3 (hereafter referred to as “Cases 12 and 32”).

SE3: $\alpha_3 = 0.0174y^{-1}$ as in Case 3 (cf. Fig. 6) is also used in Cases 1 and 2 (hereafter referred to as “Cases 13 and 23”).

Table 1 shows that the influence of a change in the exponential growth factor is small vis-à-vis the dominating influence of K and D and the quality in the estimates of T , M , and P . For instance, the dimensionless time n at $M/M_\infty = 0.5$ ranges from 15 to 19 in Case 1 and Case 1–related experiments (small persistency) and from 2 to 3 in Case 2 and Case 2–related experiments (great persistency); in Case 3 and Case 3–related experiments, it does not exhibit a range at all ($n \approx 1$; very great persistency). These ranges for n tell us how long it takes to build up 50% of the memory with time running as of $n = 0$ (1959).

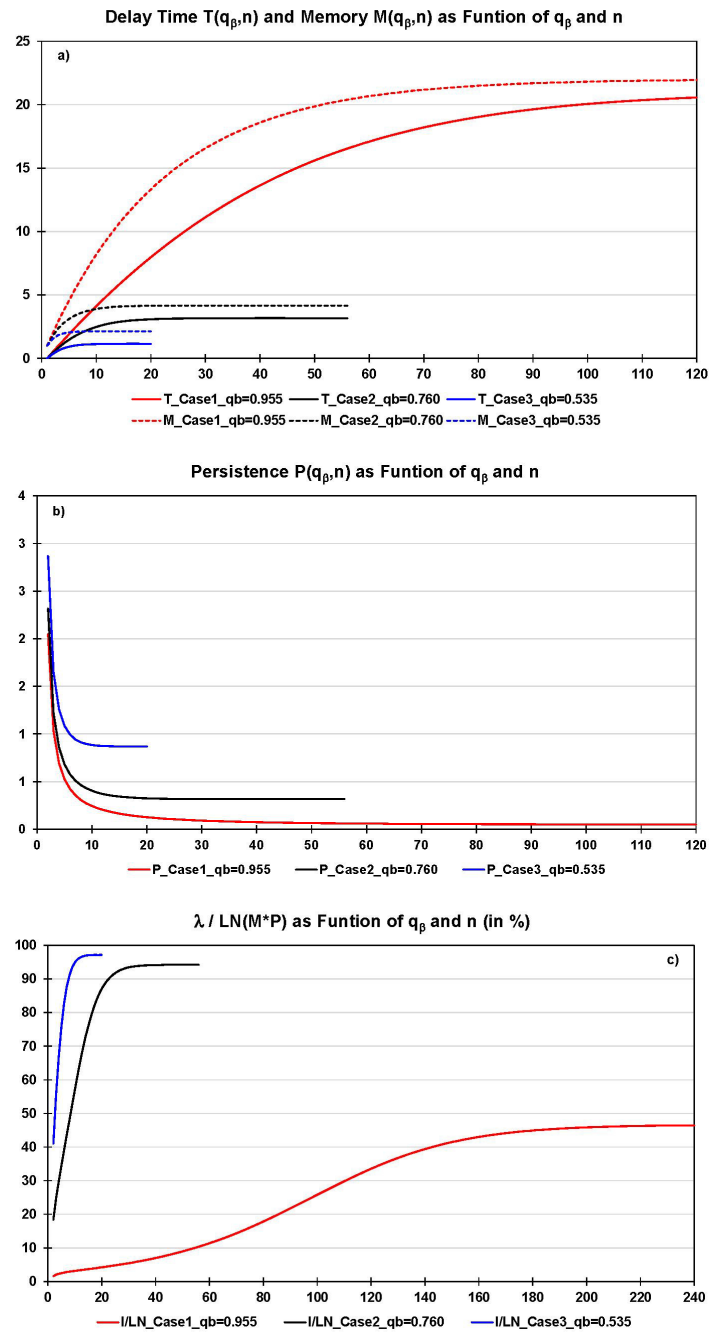


Figure 7. Cases 1–3: **a)** delay time T and memory M (in units of 1), **b)** persistence P (in units of 1), and **c)** the ratio $\lambda / \ln(M \cdot P)$ (in %); all are versus time (in units of 1) as of $n = 0$ (1959).

Table 2. Cases 1–3 and related experiments: Build-up of memory (%) as of $n = 0$ (1959).

Time		Increase in memory as of $n = 0$ (1959)		
		Cases 1, 12, 13	Cases 2, 21, 23	Cases 3, 31, 32
y	1	%	%	%
1959 ^a	0	0.0	0.0	0.0
1964	5	17–21	75–76	96
1970	11	34–40	95–96	100
2015	56	88–93	100	—

^a Start year: $\sigma_0 = \varepsilon_0 = 0$.

395 Alternatively, we can ask how much memory has been build up until a given year. Table 2 tells us that after 56 years (i.e., in
 2015) memory is still building up only in Case 1 and Case 1–related experiments, which means that the system still responds
 in its own characteristic way (as a result of a small K and a great D) to the continuously increasing stress; this is not so in
 Cases 2 and 3 (and related experiments). In the latter two cases today’s uptake of carbon by land and oceans happens de facto
 outside the system’s natural regime and solely in response to the sheer, continuously increasing stress imposed on it, whereas
 400 in Case 1 and Case 1–related experiments the limits of the natural regime are not yet reached. This interpretation of Cases 1–3
 (and related experiments) does not depend on how much carbon the system already took up before 1959. M is additive and
 defined independently of initial conditions; these only specify 1959 as reference time for $n = 0$. This means by implication
 that the current M value (or its perpetuation) is contained in the M value (or is part of that value’s perpetuation) which starts
 accruing from an earlier point in time (see also experiments B and C below).

405 Finally, it is important to note that it is prudent to expect that natural elements (like land and oceans) will not continue to
 maintain their damping (i.e., carbon uptake) capacity—or their capacity to embark on a, most likely, hysteretic downward path
 in the case of a sustained decrease in emissions—even well before they reach the limits of their natural regimes. They may
 simply collapse globally when reaching a critical threshold. We note that our choice of model binds us to the global scale and
 also does not allow “failure” to be specified further; e.g. with respect to when exactly a critical threshold will occur and in
 410 terms of whether carbon uptake decreases only or even ceases upon reaching the threshold.

To B and C

We report on the sets of stress-strain experiments B and C in combination. They can be understood as a repetition of the 1959–
 2015 Case 0 experiment (see A.1) but with the difference that now upstream emissions as of 1900 (B) or 1850 (C), respectively,
 are considered. This allows initial conditions for 1959 other than zero, as in the Case 0 experiment, to be considered (see
 415 Supplementary Information 10 and Supplementary Data 9 to 16):
 Case 0: 1959–2015

B: 1900–1958 (upstream emissions), 1959–2015

C: 1850–1958 (upstream emissions), 1959–2015

The experiments can be ordered consecutively in terms of time with the three 1959–2015 periods comprising a min–max
420 interval to facilitate the drawing of a number of robust results in spite of the uncertainty underlying these stress-strain exper-
iments (see Supplementary Information 10). Between 1850 and 1959–2015 (i) the compression modulus K increased from
 ~ 2 to 10–13 Pa (the atmosphere became less compressible) while (ii) the damping constant D decreased from ~ 468 to 459–
462 Pa y (the uptake of carbon by land and oceans became less viscous), with the consequence that (iii) the ratio $\lambda = K/D$
425 increased from ~ 0.004 – 0.005 y^{-1} to 0.021 – 0.028 y^{-1} (i.e., by a factor of 4–6). Likewise, (iv) delay time T_∞ decreased
(hence persistence P_∞ increased) from ~ 51 (~ 0.02) to 18–21 (0.047–0.055) while (v) memory M_∞ decreased from ~ 52 to
19–22 on the dimensionless time scale.

6 Account of the Findings

Here we discuss our main findings in greater depth, recollect the assumptions underlying our global stress-strain approach, and
conclude by returning to the three questions posed in the beginning.

430 We make use of a MB to model the stress-strain behaviour of the global atmosphere–land/ocean carbon system and to
simulate how humankind propelled that global-scale experiment historically, here as of 1850. The stress is given by the CO_2
emissions from fossil fuel burning and land use, while the strain is given by the expansion of the atmosphere by volume and
uptake of CO_2 by sinks. The MB is a logical choice of stress-strain model given the uninterrupted increase in atmospheric
 CO_2 concentrations since 1850.

435 The stress-strain model is unique and a valuable addendum to the suite of models (such as radiation transfer, energy balance
or box-type carbon cycle models), which are highly reduced but do not compromise complexity in principle. These models
offer great benefits in safeguarding complex three-dimensional global change models. Here too, the proposed stress-strain
approach allows three system-characteristic parameters to be distilled from the stress-explicit equation—delay time, memory,
and persistence—and new insights to be gained. What we consider most important is that these parameters come with their
440 own internal limits, which govern the behaviour of the atmosphere–land/ocean carbon system. These limits are independent
from any external target values (such as temperature targets justified by means of global change research).

Knowing these limits is precisely the reason why we can advance the discussion and draw some preliminary conclusions. To
start with, we look at the Case 0 experiment and the stress-strain experiments B and C in combination. The values of the Case 0
parameters T_∞ and M_∞ , in particular, are at the upper end of the respective 1959–2015 min–max intervals (see Supplementary
445 Information 10). That is, the respective characteristic ratios T/T_∞ and M/M_∞ reach specified levels (e.g., 0.5 or 0.95; see
Fig. 7a) slightly sooner than when T_∞ and M_∞ take on values at the lower end of the 1959–2015 min–max intervals. Given that
Case 0 is well represented by Case 1, we can use the parameter values of the latter. According to column “Case 1” in Table 1,
 M/M_∞ and T/T_∞ reached their 0.5 levels after about 15 and 28 year-equivalent units on the dimensionless time scale (which

was in 1974 and 1987), whereas they will reach their 0.95 levels after about 64 and 98 year-equivalent units (which will be in
450 2023 and 2057)—if the exponential growth factor λ remains unchanged in the future.

This not unthinkable worst case provides a reference, as follows: We understand, in particular, the ability of a system
to build up memory effectively as its ability to respond to stress still in its own characteristic way (i.e., within its natural
regime). Therefore, it appears precautionary to prefer memory over delay time in avoiding potential system failures globally
in the future. These we expect to happen well before 2050 if the current trend in emissions is not reversed immediately and
465 sustainably. However, we reiterate that our choice of model binds us to the global scale and also does not allow “failure” to be
specified further.

We consider our precautionary statement robust given both the uncertainties we dealt with in the course of our evaluation
and the restriction of our variation parameters to two. One of the two variation parameters (λ) presupposes knowing K and D
with equal inaccuracy in relative terms. This procedural measure in treating λ , in particular, offers a great applicational benefit,
460 but no serious restriction given that (while, ideally, α is constant) it is the K/D ratio that matters and whose ultimate value is
controlled by consistency—which comes in as a powerful rectifier. As a matter of fact, fulfilling consistency results in a K/D
ratio that ranges close to the lower uncertainty boundary which we deem adequate based on our preceding assessment. That is,
a smaller K : the atmosphere is more compressible than previously thought; and a greater D : the uptake of carbon by land and
oceans is more viscous than previously thought (see Cases 1–3 in Tab. 1). However, the overall effect of the continued release
465 of CO_2 emissions since 1850 on the K/D ratio is unambiguous—the ratio increased (see λ in Table SI10-2) by a factor 4–6
(K increased: the atmosphere became less compressible; D decreased: the uptake of carbon by land and oceans became less
viscous).

By way of contrast, persistence is less intelligible. Equation (5) allows persistence (as well as its systemic limit) to be
followed quantitatively. However, it is conducive to understand persistence as path dependency and in qualitative terms, i.e.
470 whether it increased or decreased. Thus, we see that P_∞ increased since 1850 by a factor of 2–3 (see P_∞ in Table SI10-2),
which indicates that the atmosphere–land/ocean system is progressively trapped from a path dependency perspective. This, in
turn, means that it will become progressively more difficult to (strain-) relax the entire system (i.e., the atmosphere including
land and oceans)—a mere 1-year decrease of a few percentage points in CO_2 emissions, as reported recently for 2020, will
have virtually no impact (Global Carbon Project, 2020).

475 To conclude, we return to the three questions posed in the beginning. These can be answered unambiguously:

Memory, just as persistence, is a characteristic (function) of the MB. Mathematically spoken, it is contained in the integral
on the right side of equation (1a) and is defined independently of initial conditions. These appear only in the lower boundary
of that integral which allows initial conditions other than zero to be considered by taking advantage of the integral’s additivity.

The memory of the atmosphere–land/ocean carbon system—Earth’s memory—can be quantified. It can be understood as
480 the depreciated strain summed up backward in time. We let memory extend backward in time to 1850, assuming zero anthro-
pogenic stress before that date. Memory is measured in units of 1 and accrues continually over time (here as the result of the
uninterrupted increase in stress).

Memory is constrained. It can be compared with a limited buffer, approximately 60% of which humankind had already exploited prior to 1959 (see M_∞ in Tab. SI10-2). We understand the effective build-up of memory as Earth's ability to respond still within its own natural stress-strain regime. However, this ability declines considerably with memory reaching high levels of exploitation (see $M/M_\infty \geq 0.95$ in Table 1)—which we anticipate happening in the foreseeable future if CO₂ emissions continue to increase globally as before.

Finally, we can also quantify the persistence of the atmosphere–land/ocean carbon system. It is also measured in units of 1. Persistence can be understood intuitively as path dependency and in qualitative terms. Concomitantly with the exploitation of memory, we see that P_∞ increased since 1850 by approximately a factor 2–3—and can be expected to increase further if the release of CO₂ emissions globally continues as before.

Based on these stress-strain insights we expect that the atmosphere–land/ocean carbon system is forced outside its natural regime well before 2050 if the current trend in emissions is not reversed immediately and sustainably.

Data availability. Supplementary Material (Supplementary Information and Supplementary Data): <https://doi.org/10.22022/em/06-2021>.
123

Author contributions. M. J. set up the physical model of the atmosphere–land/ocean system; derived its delay time, memory, and persistence; and provided the initial estimates of its compression and damping characteristics. R. B. contributed to the physical and mathematical improvement of the method and the physical consistency of results. I. R. and P. Z. contributed to the inspection of mathematical relations globally and their generalizations. P. Z. contributed to the strengthening of the method by evaluating alternative memory concepts known in mathematics.

Acknowledgements. Funding was provided by the authors' home institutions. Additional funding to facilitate collaboration between the Lviv Polytechnic National University and IIASA was provided by the bilateral Agreement on Scientific and Technological Co-operation between the Cabinet of Ministers of Ukraine and the Government of the Republic of Austria (S&T Cooperation Project 10/2019; <https://oead.at/en/> and www.mon.gov.ua/). Net primary production, land-use change emission, and atmospheric expansion data were kindly provided personally by Michael O'Sullivan (University of Exeter), Julia Pongratz (Ludwig Maximilian University of Munich), and Andrea K. Steiner (Wegener Center for Climate and Global Change, Graz).

References

- Abshire, J. B., Riris, H., Allan, G. R., Weaver, C. J., Mao, J., Sun, X., Hasselbrack, W. E., Kawa, S. R., and Biraud, S.: Pulsed airborne lidar measurements of atmospheric CO₂ column absorption, *Tellus B*, 62(5), 770–783, <https://doi.org/10.1111/j.1600-0889.2010.00502.x>, 2010.
- Aghabozorgi, S., Shirkhorshidi, A. S., and Wah, T. Y.: Time-series clustering – a decade review, *Inform. Syst.*, 53, 16–38, <https://doi.org/10.1016/j.is.2015.04.007>, 2015.
- Amthor, J. S., and Koch, G. W.: Biota growth factor β : stimulation of terrestrial ecosystem net primary production by elevated atmospheric CO₂, in: *Carbon Dioxide and Terrestrial Ecosystems*, edited by: Koch, G. W., and Mooney, H. A., Academic Press, San Diego, United States of America, 399–414, 1996.
- Barros, C. P., Gil-Alana, L. A., and Perez de Gracia, F.: Stationarity and long range dependence of carbon dioxide emissions: evidence for disaggregated data, *Environ. Resource Econ.*, 63, 45–56, <https://doi.org/10.1007/s10640-014-9835-3>, 2016.
- Bates, N. R., Astor, Y. M., Church, M. J., Currie, K., Dore, J. E., González-Dávila, M., Lorenzoni, L., Muller-Karger, F., Olafsson, J., and Santana-Casiano, J. M.: A time-series view of changing ocean chemistry due to ocean uptake of anthropogenic CO₂ and ocean acidification, *Oceanography*, 27, 126–141, <https://doi.org/10.5670/oceanog.2014.16>, 2014.
- Belbute, J. M., and Pereira, A. M.: Do global CO₂ emissions from fossil-fuel consumption exhibit long memory? A fractional integration analysis, *Appl. Econ.*, 4055–4070, <https://doi.org/10.1080/00036846.2016.1273508>, 2017.
- Bertram, A., and Glüge, R.: Festkörpermechanik: Einachsige Materialtheorie: Viskoelastizität: Der MAXWELL-Körper, Otto-von-Guericke University Magdeburg, Germany, <https://docplayer.org/11977674-Festkoerpermechanik-mit-beispielen-von-albrecht-bertram-von-rainer-gluege-otto-von-guericke-universitaet-magdeburg.html>, 2015.
- Boucher, O., Halloran, P. R., Burke, E. J., Doutriaux-Boucher, M., Jones, C. D., Lowe, J., Ringer, M. A., Robertson, E., and Wu, P.: Reversibility in an Earth system model in response to CO₂ concentration changes, *Environ. Res. Lett.*, 7, 24013 (9pp), <https://doi.org/10.1088/1748-9326/7/2/024013>, 2012.
- Caballero, R., Jewson, S., and Brix, A.: Long memory in surface air temperature: Detection, modeling, and application to weather derivative valuation, *Clim. Res.*, 21, 127–140, <https://doi.org/10.3354/cr021127>, 2002.
- CarbonBrief: Climate modelling. Q&A: How do climate models work? <https://www.carbonbrief.org/qa-how-do-climate-models-work> (last access 28 January 2022), 15 January 2018.
- Cavcar, M.: The international standard atmosphere (ISA), Anadolu University, Eskişehir, Turkey (7pp), <http://fisicaatmo.at.fcen.uba.ar/practicas/ISAweb.pdf>, 2000.
- Darlington, R. B.: A regression approach to time-series analysis, Script, Cornell University, Ithaca NY, United States of America, <http://node101.psych.cornell.edu/Darlington/series/series0.htm>, 1996.
- Darlington, R. B., and Hayes, A. F.: *Regression analysis and linear models: Concepts, Applications, and Implementation*, The Guilford Publications, New York NY, United States of America, <https://www.guilford.com/books/Regression-Analysis-and-Linear-Models/Darlington-Hayes/9781462521135>, 2016.
- Digital Dutch: 1976 Standard atmosphere calculator, <https://www.digitaldutch.com/atmoscalc/> (last access 28 January 2022), 1999.
- Dusza, Y., Sanchez-Cañete, E. P., Le Galliard, J.-F., Ferrière, R., Chollet, S., Massol, F., Hansart, A., Juarez, S., Dontsova, K., van Haren, J., Troch, P., Pavao-Zuckerman, M. A., Hamerlynck, E., and Barron-Gafford, G. A.: Biotic soil-plant interaction processes explain most of

- hysteric soil CO₂ efflux response to temperature in cross-factorial mesocosm experiment, *Sci. Rep.*, 10, 905 (11pp), <https://doi.org/10.1038/s41598-019-55390-6>, 2020.
- 545 Egleston, E. S., Sabine, C. L., and Morel, F. M. M.: Revelle revisited: buffer factors that quantify the response of ocean chemistry to changes in DIC and alkalinity, *Glob. Biochem. Cycles*, 24, GB1002 (9pp), <https://doi.org/10.1029/2008GB003407>, 2010.
- Emerson, S. and Hedges, J.: *Chemical Oceanography and the Marine Carbon Cycle*, Cambridge University Press, Cambridge NY, United States of America, <https://slideplayer.com/slide/9820843/> (PDF overview of Section 4.4 by Ford, C., Lecture 10: Ocean Carbonate Chemistry: Ocean Distributions), 2008.
- 550 Emmert, J. T., Stevens, M. H., Bernath, P. F., Drob, D. P., and Boone, C. D.: Observations of increasing carbon dioxide concentration in Earth's thermosphere, *Nat. Geosci.*, 5, 868–871, <https://www.nature.com/articles/ngeo1626>, 2012 (background source to <https://phys.org/news/2012-11-atmospheric-co2-space-junk.html>; last access 28 January 2022).
- Flato, G., Marotzke, J., Abiodun, B., Braconnot, P., Chou, S. C., Collins, W., Cox, P., Driouech, F., Emori, S., Eyring, V., Forest, C., Gleckler, P., Guilyardi, E., Jakob, C., Kattsov, V., Reason, C., and Rummukainen, M.: Evaluation of climate models, in: *Climate Change 2013: The Physical Science Basis. Contribution of Working Group I to the Fifth Assessment Report of the Intergovernmental Panel on Climate Change*, edited by Stocker, T. F., Qin, D., Plattner, G.-K., Tignor, M., Allen, S. K., Boschung, J., Nauels, A., Xia, Y., Bex, V., and Midgley, P. M., Cambridge University Press, Cambridge, United Kingdom, 741–866, https://www.ipcc.ch/site/assets/uploads/2018/02/WG1AR5_Chapter09_FINAL.pdf, 2013.
- 555 Franzke, C.: Long-range dependence and climate noise characteristics of Antarctic temperature data, *J. Climate*, 23(22), 6074–6081, <https://doi.org/10.1175/2010JCLI3654.1>, 2010.
- Garbe, J., Albrecht, T., Levermann, A., Donges, J. F., and Winkelmann, R.: The hysteresis of the Antarctic ice sheet, *Nature*, 585, 538–544, <https://doi.org/10.1038/s41586-020-2727-5>, 2020.
- Global Carbon Project: Global carbon budget 2019, <https://www.icos-cp.eu/science-and-impact/global-carbon-budget/2019>, 4 December 2019 (published together with other original peer-reviewed papers and data sources).
- 565 Global Carbon Project: Carbon budget 2020, <https://www.icos-cp.eu/science-and-impact/global-carbon-budget/2020>, 11 December 2020 (published together with other original peer-reviewed papers and data sources).
- Harman, I. N., and Trudinger, C. M.: The simple carbon-climate model: SCCM7, CAWCR Technical Report No. 069, https://www.cawcr.gov.au/technical-reports/CTR_069.pdf, 2014.
- 570 Heimann, M., and Reichstein, M.: Terrestrial ecosystem carbon dynamics and climate feedbacks, *Nature*, 451, 289–292, <https://doi.org/10.1038/nature06591>, 2008.
- International Organization for Standardization: Standard atmosphere, ISO 2533:1975, 1975 (background source to https://en.wikipedia.org/wiki/International_Standard_Atmosphere; last access: 28 January 2022).
- Lackner, B. C., Steiner, A. K., Hegerl, G. C., and Kirchengast, G.: Atmospheric climate change detection by radio occultation using a fingerprinting method, *J. Climate*, 24, 5275–5291, <https://doi.org/10.1175/2011JCLI3966.1>, 2011.
- 575 Lüdecke H. J., Hempelmann, A., and Weiss, C. O.: Multi-periodic climate dynamics: spectral analysis of long-term instrumental and proxy temperature records, *Clim. Past*, 9, 447–452, <https://doi.org/10.5194/cp-9-447-2013>, 2013.
- Luo, Y., and Mooney, H. A.: Stimulation of global photosynthetic carbon influx by an increase in atmospheric carbon dioxide concentration, in: *Carbon Dioxide and Terrestrial Ecosystems*, edited by Koch, G. W., and Mooney, H. A., Academic Press, San Diego, United States of America, 381–397, 1996.
- 580 Malkin, A. Ya., and Isayev, A. I.: *Rheology: Concepts, Methods, and Applications*, ChemTech Publishing, Toronto, Canada, 2017.

- Mezger, T. G.: The Rheology Handbook, Vincentz Network, Hannover, Germany, <https://www.researchgate.net/profile/Abdelkader-Bouaziz/post/Technical-standard-for-the-determination-of-resin-viscosity/attachment/5c180653cfe4a7645509c278/AS%3A704923863900166%401545078354412/download/The+Rheology+Handbook+-+For+Users+of+Rotational.pdf>, 2006 (background source to <https://de.wikipedia.org/wiki/Viskosit%C3%A4t>; last access 28 January 2022).
- 585 Mohanakumar, K.: Structure and composition of the lower and middle atmosphere, in: *Stratosphere Troposphere Interactions*, 1–53, Springer, https://doi.org/10.1007/978-1-4020-8217-7_1, 2008.
- Müller, G.: Generalized Maxwell bodies and estimates of mantle viscosity, *Geophys. J. Int.*, 87(3), 1113–1141, <https://doi.org/10.1111/j.1365-246X.1986.tb01986.x>, 1986.
- 590 NASA Earth Observatory: The top of the atmosphere, <https://earthobservatory.nasa.gov/images/7373/the-top-of-the-atmosphere> (last access 28 January 2022), 2006.
- National Oceanic and Atmospheric Administration: Science on a sphere: ocean-atmosphere CO₂ exchange, NOAA Global Systems Division, Boulder CO, United States of America, <https://sos.noaa.gov/datasets/ocean-atmosphere-co2-exchange/> (last access 28 January 2022), 2015.
- 595 OpenStax: Stress, strain, and elastic modulus (Part 2), <https://phys.libretexts.org/@go/page/6472> (last access 28 January 2022), 5 November 2020.
- O’Sullivan, M., Spracklen, D. V., Batterman, S. A., Arnold, S. R., Gloor, M., and Buermann, W.: Have synergies between nitrogen deposition and atmospheric CO₂ driven the recent enhancement of the terrestrial carbon sink? *Global Biogeochem. Cycles*, 33, 163–180, <https://doi.org/10.1029/2018GB005922>, 2019.
- 600 Philipona, R., Mears, C., Fujiwara, M., Jeannot, P., Thorne, P., Bodeker, G., Haimberger, L., Hervo, M., Popp, C., Romanens, G., Steinbrecht, W., Stübi, R., and Van Malderen, R.: Radiosondes show that after decades of cooling, the lower stratosphere is now warming, *J. Geophys. Res. Atmos.*, 123, 12,509–12,522, <https://doi.org/10.1029/2018JD028901>, 2018.
- Roylance, D.: Engineering viscoelasticity, Massachusetts Institute of Technology, Cambridge MA, United States of America, <http://web.mit.edu/course/3/3.11/www/modules/visco.pdf>, 24 October 2001.
- 605 Sakazaki, S., and Hamilton, K.: An array of ringing global free modes discovered in tropical surface pressure data, *J. Atmos. Sci.*, 77, 2519–2530, <https://doi.org/10.1175/JAS-D-20-0053.1>, 2020 (background source to <https://physicsworld.com/a/earths-atmosphere-rings-like-a-giant-bell-say-researchers/>; last access 28 January 2022).
- Schwinger, J., and Tjiputra, J.: Ocean carbon cycle feedbacks under negative emissions, *Geophys. Res. Lett.*, 45, 5062–5070, <https://doi.org/10.1029/2018GL077790>, 2018.
- 610 Smith, P.: Soils and climate change, *Curr. Opin. Environ. Sust.*, 4, 539–544, <https://doi.org/10.1016/j.cosust.2012.06.005>, 2012.
- Steiner, A. K., Lackner, B. C., Ladstädter, F., Scherllin-Pirscher, B., Foelsche, U., and Kirchengast, G.: GPS radio occultation for climate monitoring and change detection, *Radio Sci.*, 46, RS0D24 (17pp), <https://doi.org/10.1029/2010RS004614>, 2011.
- Steiner, A. K., Ladstädter, F., Randel, W. J., Maycock, A. C., Fu, Q., Claud, C., Gleisner, H., Haimberger, L., Ho, S.-P., Keckhut, P., Leblanc, T., Mears, C., Polvani, L. M., Santer, B. D., Schmidt, T., Sofieva, V., Wing, R., and Zou, C.-Z.: Observed temperature changes in the troposphere and stratosphere from 1979 to 2018, *J. Climate*, 33, 8165–8194, <https://doi.org/10.1175/JCLI-D-19-0998.1>, 2020.
- 615 Steffen, W., Richardson, K., Rockström, J., Cornell, S. E., Fetzer, I., Bennett, E. M., Biggs, R., Carpenter, S. R., de Vries, W., de Wit, C. A., Folke, C., Gerten, D., Heinke, J., Mace, G. M., Persson, L. M., Ramanathan, V., Reyers, B., and Sörlin, S.: Planetary boundaries: guiding human development on a changing planet, *Science*, 347, 6223, 1259855, <https://www.science.org/doi/epdf/10.1126/science.1259855>, 2015.

- 620 Steffen, W., Sanderson, A., Tyson, P., Jäger, J., Matson, P., Moore, B. III, Oldfield, F., Richardson, K., Schellnhuber, H. J., Turner, B. L. II, and Wasson, R. J.: *Global Change and the Earth System: A Planet Under Pressure*, Springer-Verlag, Berlin, Germany, <http://www.igbp.net/publications/igbpbookseries/igbpbookseries/globalchangeandtheearthsystem2004.5.1b8ae20512db692f2a680007462.html>, 2004.
- TU Delft: Rheometer. Faculty of Civil Engineering and Geosciences, Delft, The Netherlands, <https://www.tudelft.nl/en/ceg/about-faculty/departments/watermanagement/research/waterlab/equipment/rheometer> (last access 28 January 2022).
- 625 UN Climate Change: The Paris Agreement, <https://unfccc.int/process-and-meetings/the-paris-agreement/the-paris-agreement> (last access 28 January 2022).
- UN Sustainable Development Goals: The Sustainable Development Agenda, <https://www.un.org/sustainabledevelopment/development-agenda/> (last access 28 January 2022)
- Wark, K.: *Thermodynamics*, McGraw2Hill, New York NY, United States of America, 1983 (background source to http://homepages.wmich.edu/~cho/ME432/Appendix1_SIunits.pdf; cf. also https://en.wikipedia.org/wiki/Heat_capacity_ratio; last access 28 January 2022)
- 630 Whitehouse, P. L., Gomez, N. King, M. A., and Wiens, D. A.: Solid Earth change and the evolution of the Antarctic Ice Sheet, *Nat. Commun.*, 10, 503 (14pp), <https://doi.org/10.1038/s41467-018-08068-y>, 2019.
- Wullschleger, S. D., Post, W. M., and King, A. W.: On the potential for a CO₂ fertilization effect in forests: estimates of the biotic growth factor based on 58 controlled-exposure studies, in: *Biotic Feedbacks in the Global Climatic System*, edited by: Woodwell, G. M., and Mackenzie, F. T., Oxford University Press, New York NY, United States of America, 85–107, 1995.
- 635 Yuen, D. A., Sabadini, R. C. A., Gasperini, P., and Bisch, E.: On transient rheology and glacial isostasy, *J. Geophys. Res.*, 91, B11, 11,420–11,438, <https://doi.org/10.1029/JB091iB11p11420>, 1986.
- Zellner, R.: Die Atmosphäre – Zwischen Erde und Weltall: Unsere lebenswichtige Schutzhülle, in: *Chemie über den Wolken . . . und darunter*, edited by Zellner, R., and Gesellschaft Deutscher Chemiker e.V., Wiley-VCH Verlag, Weinheim, Germany, 8–17, https://application.wiley-vch.de/books/sample/3527326510_c01.pdf, 2011.
- 640